Research Article Vol. 32, No. 21 / 7 Oct 2024 / Optics Express 37148
Optics EXPRESS

Burst-mode digital signal processing for passive optical networks based on discrete multi-tone

JI ZHOU,[1,*] ZHIYANG LIU,[1] MENGQI GUO,[2] HAIDE WANG,[3] WEIPING LIU,[1] AND CHANGYUAN YU[4]

[1]Department of Electronic Engineering, College of Information Science and Technology, Jinan University, Guangzhou 510632, China
[2]School of Information Science and Technology, Shijiazhuang Tiedao University, Shijiazhuang 050043, China
[3]School of Cyber Security, Guangdong Polytechnic Normal University, Guangzhou 510665, China
[4]Department of Electrical and Electronic Engineering, The Hong Kong Polytechnic University, Hong Kong SAR, China
[*]zhouji@jnu.edu.cn

Abstract: Driven by the ever-increasing capacity demands, digital signal processing (DSP) has been first applied to improve the performance of a 50G passive optical network (PON). The main challenge is implementing the burst-mode DSP to deal with the upstream burst signal. This paper proposes a burst-mode DSP using preambles designed for the 50G PON based on entropy-loading discrete multi-tone (DMT). The burst-mode DSP mainly includes the burst-mode timing recovery with the initial timing offset and the burst-mode frequency-domain equalizer with the initial tap coefficients. The experimental results of the 50G DMT PON demonstrate that the burst-mode DSP can achieve fast convergence based on the ~27ns preamble with 800 samples. The proposed burst-mode DSP makes the DMT PON highly feasible to support non-residential point-to-multi-point applications such as passive optical local area networks.

1. Introduction

In recent years, the development of optical access networks has been driven by artificial intelligence, cloud services, high-definition video, and so on [1–3]. The International Telecommunication Union's Telecommunication Standardization Sector (ITU-T) has released the standards for 50G passive optical network (50G PON) to meet the ever-increasing capacity demands. To ensure the optical power budget, the 50G PON still use on-off keying and first adopt digital signal processing (DSP) [4–6]. Many non-residential applications of PON such as passive optical local area networks do not require a high optical power budget but are cost-sensitive, which is preferred to low-cost bandwidth-limited devices. Spectral-efficient discrete multi-tone (DMT) enables the use of low-cost bandwidth-limited devices, which is a promising scheme for the non-residential point-to-multi-point (P2MP) applications of 50G PON [7–9].

Since the beginning of the PON commercial applications, statistical-multiplexing time division multiple access (TDMA) has been used to ensure capacity and quantity for the subscribers [4,10]. In the new 50G TDM-PON, burst-mode DSP is one of the key technologies to deal with the upstream burst signal, which should have a short convergence time to improve spectral efficiency [11,12]. Among the conventional DSP modules, the timing recovery and channel equalization with feedback updating algorithms have long convergence times, which are not suitable for processing the upstream burst signal. Therefore, many efforts have been committed to the burst-mode timing recovery (TR) and channel equalizer for the 50G PON [13–18]. Most of the existing burst-mode DSP has addressed the requirements for processing single-carrier burst signals such as on-off keying and four-level pulse amplitude modulation. The burst-mode

#538190 https://doi.org/10.1364/OE.538190
Journal © 2024 Received 31 Jul 2024; revised 18 Sep 2024; accepted 23 Sep 2024; published 30 Sep 2024

Optics EXPRESS

DSP for processing multi-carrier burst signals such as DMT is further studied to promote P2MP applications.

In this paper, we propose the burst-mode DSP based on the designed preambles for the 50G DMT PON, including burst-mode TR with timing offset initialization and burst-mode frequency-domain equalizer (FDE) with tap coefficients initialization. The initial timing offset can be extracted by the feedforward timing offset estimation based on the designed frequency tones. Then, the initial tap coefficients can be estimated by the minimum-mean-square-error (MMSE)-based channel estimation based on the known DMT-based preambles. The experimental results of the 50G DMT PON demonstrate that the proposed burst-mode DSP can realize fast convergence using ~ 27ns (i.e., 800 samples/30GSa/s) preambles. The proposed burst-mode DSP makes the DMT PON more competitive for non-residential P2MP applications.

2. Principle of burst-mode DSP

Figure 1(a) shows the frame structure and designed preambles for the DMT PON. The preambles are added before the payload for fast convergence of the burst-mode DSP. The Preamble A is designed as two conjugate tones on the symmetry frequency points to estimate the initial timing offset. The length of the Preamble A is set to 128. The Preamble B is designed for frame synchronization, which has been demonstrated in Refs. [19,20]. The length of the Preamble B is set to 128. Figure 1(b) depicts the detailed structure of Preamble C to estimate the initial tap coefficients. The Preamble C consists of four known DMT symbols [$\mathbf{S}_{C1}$ $\mathbf{S}_{C2}$ $\mathbf{S}_{C3}$ $\mathbf{S}_{C4}$] with cyclic prefix (CP) and cyclic suffix (CS). The length of the Preamble C is set to 544. In conclusion, the total length of the preambles is 800, which can be used to realize the fast convergence of burst-mode DSP.

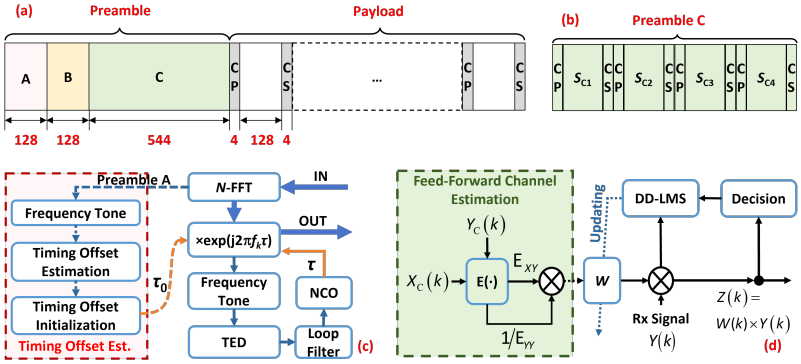

Fig. 1. (a) The frame structure and designed preambles for the DMT PON. (b) The detailed structure of Preamble C. (c) Burst-mode TR with the initial timing offset extracted by feedforward timing offset estimation based on the Preamble A. (d) Burst-mode FDE with initial tap coefficients estimated by feedforward channel estimation based on the Preamble C. NCO: Numerically Controlled Oscillator.

Next, we will introduce the principles of the burst-mode TR and burst-mode FDE. The burst-mode TR and burst-mode FDE work at a sample rate of 1 sample per symbol. The frequency-domain $Y(k)$ of the received signal can be expressed as

$$Y(k) = X(k) \times H(k) \times \exp(-j\frac{2\pi}{K}k\tau) + N(k) \tag{1}$$

where $\mathbf{X}$ is the frequency-domain transmitted signal. $\mathbf{H}$ is the frequency-domain channel response. K is the size of the fast Fourier transform (FFT). k is the subcarrier index from 0 to $K-1$. τ is

Optics EXPRESS

the timing offset. **N** is the white noise. The burst-mode TR and burst-mode FDE are proposed to compensate for timing offset τ and channel response $H(k)$, respectively.

In the burst-mode TR, an appropriate initial timing offset plays a significant role in the algorithm convergence [19,20]. Figure 1(c) shows the burst-mode TR with the initial timing offset extracted by feedforward timing offset estimation based on the Preamble A. First of all, the frequency tones of Preamble A are recognized by the frame detection. Then, the initial timing offset τ_0 is extracted by feedforward timing offset estimation, which can be expressed as

$$\tau_0 = -\frac{K}{2\pi k_0} \times \arg[Y_{\mathrm{A}}(k_0)] \tag{2}$$

where $\arg(\cdot)$ denotes the angle of a complex value. $\mathbf{Y}_{\mathrm{A}}$ is the frequency-domain received Preamble A. k_0 is the subcarrier index where the positive frequency tone is located. As Eq. (1) shows, it is worth noting that the phase-frequency response of **H** causes the estimation error on τ_0. Since the phase-frequency response of the channel in low frequency is stable [21], the relative-low frequency tones can be used for timing recovery.

After timing offset initialization, the timing offset can be preliminarily compensated by multiplying the k-th subcarrier by the $\exp(j2\pi f_k \tau_0)$. However, the timing offset τ is dynamically changed, which should always be tracked and updated. The updating timing offset τ can be estimated by a new frequency-domain timing error detection (TED) as

$$OUT_{\mathrm{TED}} = -2 \times \mathrm{Real}[Y(k_0)] \times \mathrm{Imag}[Y(k_0)] = \sin(\pi\tau) \tag{3}$$

where $\mathrm{Real}(\cdot)$ denotes the real part of a complex value. $\mathrm{Imag}(\cdot)$ denotes the imaginary part of a complex value. The loop delay should be considered when tracking timing offset based on the Eq. (3). Therefore, the initial timing offset is necessary to accelerate the convergence of the TR algorithm. The timing offset of the DMT signal can be compensated by multiplying the k-th subcarrier by the $\exp(j2\pi f_k \tau)$.

After TR, the frame synchronization is realized using Preamble B. Next, the principle of the burst-mode FDE with the initial tap coefficients will be introduced to compensate for the channel response. Figure 1(d) shows burst-mode FDE with initial tap coefficients estimated by feedforward channel estimation based on the Preamble C. First of all, the mean square error (MSE) of the Preamble C is calculated by

$$e(k) = [X(k) - Y(k) \times W_{\mathrm{Est}}(k)]^2 \tag{4}$$

where $\mathbf{W}_{\mathrm{Est}}$ denotes the estimated tap coefficients. Most of the channel estimations aim to obtain the $\mathbf{W}_{\mathrm{Est}}$ to minimize the MSE, including the feedback and feedforward algorithms. Due to the loop delay, the feedback channel estimation requires a long convergence time. The feedforward zero-forcing (ZF)-based and MMSE-based channel estimations can quickly obtain the initial tap coefficients. The ZF-based channel estimation owns a simplified implementation [22], which can be directly calculated by dividing the transmitted Preamble C by the received Preamble C in the frequency domain. The initial tap coefficients estimated by the ZF-based channel estimation can be defined as

$$W_{\mathrm{ZF}}(k) = \frac{X_{\mathrm{C}}(k)}{Y_{\mathrm{C}}(k)} = \frac{1}{H(k) + N(k)/X_{\mathrm{C}}(k)} \tag{5}$$

where $\mathbf{W}_{\mathrm{ZF}}$ denotes the estimated tap coefficients by ZF-based channel estimation. $\mathbf{X}_{\mathrm{C}}$ and $\mathbf{Y}_{\mathrm{C}}$ denote the transmitted and received Preamble C, respectively. From Eq. (5), the main drawback is that the ZF-based channel estimation is vulnerable to noise. The four $\mathbf{W}_{\mathrm{ZF}}$ estimated by the four known DMT symbols in Preamble C are averaged to improve the accuracy.

In the MMSE-based channel estimation, the tap coefficients are calculated by setting the gradient value of MSE to zero. Compared to the ZF-based channel estimation, the MMSE-based

Optics EXPRESS

channel estimation can mitigate the influence of noise on the tap coefficients [23], which can be defined as

$$W_{\mathrm{MMSE}}(k) = \frac{\mathrm{E}[X_{\mathrm{C}}(k) \times Y_{\mathrm{C}}^{*}(k)]}{\mathrm{E}[Y_{\mathrm{C}}(k) \times Y_{\mathrm{C}}^{*}(k)]} \tag{6}$$

where $\mathrm{E}(\cdot)$ denotes the expectation operation for the correlation values calculated by four known DMT symbols in Preamble C. $(\cdot)^{*}$ denotes the conjugate operation.

After the feedforward channel estimation, the tap coefficients are fed into the burst-mode FDE. The channel response can be preliminarily compensated by multiplying the k-th subcarriers by the $W_{\mathrm{ZF}}(k)$ or $W_{\mathrm{MMSE}}(k)$. However, the channel response is dynamically changed, which should always be tracked and updated. The tap coefficients $\mathbf{W}_{\mathrm{Upd}}$ can be updated by the decision-directed least mean square (DD-LMS) algorithm, which can be expressed as

$$W_{\mathrm{Upd}}(k) = W(k) - \mu\xi(k) \tag{7}$$

where μ is the step size. $\xi(k)$ is a gradient value of MSE in Eq. (4), which can be expressed as

$$\xi(k) = -2 \times [\hat{Z}(k) - Y(k) \times W(k)] \times Y(k) \tag{8}$$

where $\hat{Z}(k)$ is the direct-decision value of equalized signal $Z(k)$. Both the MMSE-based channel estimation and the DD-LMS updating algorithm are based on the criterion of minimizing the MSE between the transmitted signal and the equalized signal. Therefore, in theory, the MSE has a small fluctuation when the MMSE-based channel estimation is switched to the DD-LMS updating algorithm.

3. Experimental setups and results

An experiment of 50Gb/s entropy-loading DMT PON was set up to verify the feasibility of the proposed burst-mode DSP. Figure 2(a) shows the experimental setups of the 50Gb/s entropy-loading DMT PON. Firstly, the DSP at the transmitter (Tx) (Tx DSP) generated the DMT signal, as depicted in Fig. 2(b). The number of symbols in the payload and the size of FFT are set to 700 and 128, respectively. The valid subcarrier number was set to 106 among the 128 subcarriers. The digital DMT signal was converted to an analog signal by a digital-to-analog converter (DAC) with a 3dB bandwidth of 16GHz. The sampling rate of DAC was set to 30GSa/s. An electrical amplifier amplified the analog signal. Then, the amplified analog signal was modulated on a 1328nm optical carrier by a 10G-class transmitter optical subassembly (TOSA) with a directly modulated laser (DML).

Figure 2(c) shows the spectrum of the transmitted signal and the received signal. To satisfy the demand of Hermitian conjugate, a pair of real-valued frequency tones was inserted on the 33rd subcarrier and 97th subcarrier. If complex frequency tones are used, the phase of the transmitted signal will affect the estimated timing error. Thus, the complex frequency tones are not suitable for the proposed timing recovery algorithm. The power ratio of the frequency tones to the symbol power of the effective carrier is 1. Figure 2(d) shows the entropies of the subcarriers. When probabilistic shaping 64-order quadrature amplitude modulation (PS-64QAM) was used, the entropies of the valid subcarriers can be set between 2 bits/symbol and 6 bits/symbol after the entropy loading. In the ITU-T standard of 50G PON, the line rate is defined as 50Gb/s, which mainly includes preambles, payloads, and a 20% forward error correction (FEC) overhead. The average entropy of the valid subcarriers was set to ~ 3.95 bits/symbol to achieve the same net rate as using on-off keying in the of the 50G passive optical network [24–26].

The optical signal was then launched into 20km standard single-mode fiber (SSMF) with the launch optical power of ~ 3dBm. A variable optical attenuator (VOA) was used at the receiver to adjust the received optical power (ROP). A 10G-class receiver optical subassembly (ROSA) with the avalanche photo-diode with a trans-impedance amplifier (APD-TIA) was used to

Optics EXPRESS

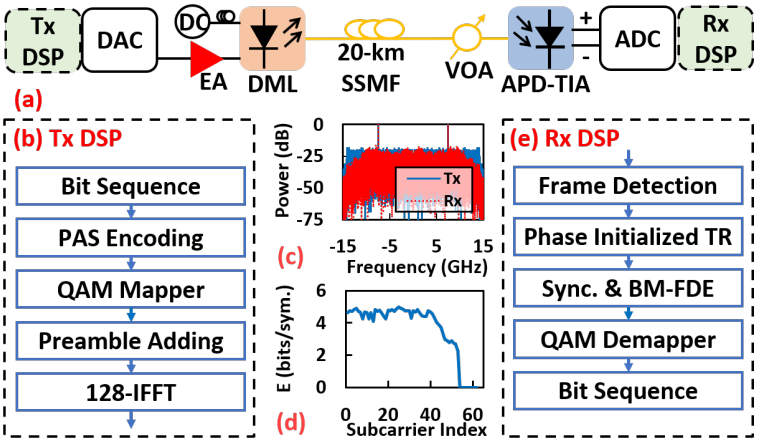

Fig. 2. (a) Experimental setups of 50Gb/s entropy-loading DMT PON. (b) Tx DSP. (c) The DMT signal spectrum. (d) The entropies on subcarriers. (e) Rx DSP. PAS: Probabilistic amplitude shaping. BM: Burst mode. Sync: Synchronization.

convert the optical signal to an electrical signal. The electrical signal was then sent to a 30GSa/s analog-to-digital converter (ADC) to convert the analog signal to a digital signal. Finally, the DSP at the receiver (Rx DSP) was used to recover the digital signal, as shown in Fig. 2(e).

Figures 3(a) and (b) show the estimated timing offset by the TR with and without the timing offset initialization under the timing frequency and jitter offset, respectively. Due to the loop delay, the timing offsets estimated by TR have a fixed delay compared to the added timing offset. The burst-mode TR uses Preamble A with 128 samples to estimate the initial timing offset. Using the initial timing offset, the burst-mode TR can track the timing offset rapidly under the timing frequency and jitter offset. The TR without timing offset initialization required more symbols to track the timing offset under the timing frequency and jitter offset. The DMT symbols within tracking time have worse performance than those within converged time. Therefore, the burst-mode TR with timing offset initialization has better performance than that without timing offset initialization within tracking time.

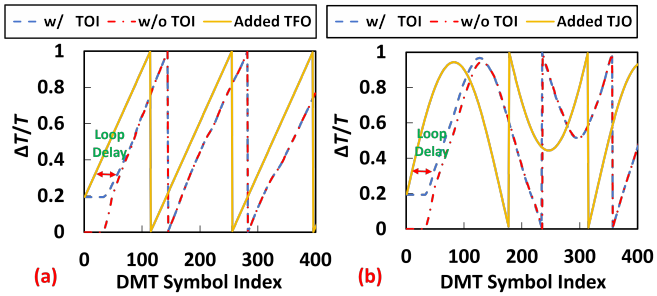

Fig. 3. The estimated timing offset by the TR with and without the timing offset initialization (TOI) under (a) the timing frequency offset (TFO) and (b) the timing jitter offset (TJO).

Figures 4(a) and (b) show the average MSE of all active subcarriers using the DD-LMS updating algorithm with initial tap coefficients based on ZF-based and MMSE-based channel estimations, respectively when the ROP is set to −17dBm after 20km SSMF transmission. The DD-LMS updating algorithm is performed after the channel estimation. When the ZF-based channel estimation is used to obtain the initialized tap coefficients, the FDE with the DD-LMS updating

Optics EXPRESS

algorithm requires a longer convergence time. This is because the ZF-based channel estimation does not consider the noise distribution leading to limited accuracy and weak noise robustness. When the initial tap coefficients are estimated by the MMSE-based channel estimation, the FDE with the DD-LMS updating algorithm has a shorter convergence time.

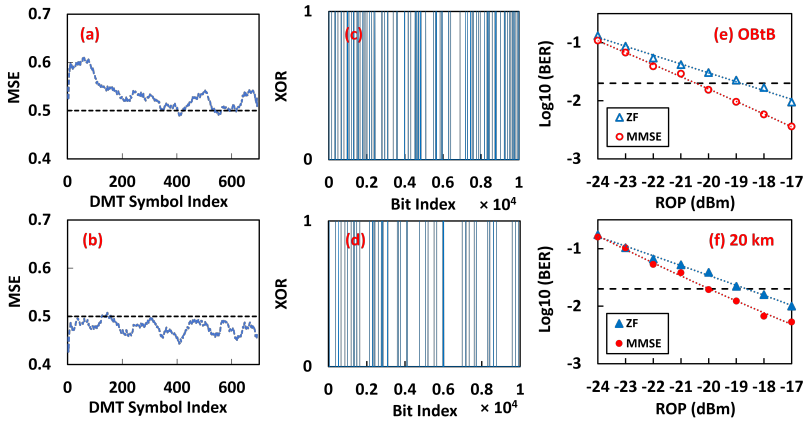

Fig. 4. The average MSE using DD-LMS updating algorithm with initial tap coefficients using (a) ZF-based and (b) MMSE-based channel estimations. Bit error distribution using (c) ZF-based and (d) MMSE-based channel estimations. BER versus ROP of the first 10^4 bits using the ZF-based and MMSE-based channel estimations after (e) OBtB and (f) 20km SSMF. The dashed lines denote the 20% FEC limit.

Figures 4(c) and (d) show the bit error distributions of the first 10^4 bits using ZF-based and MMSE-based channel estimations, respectively. Due to the loop delay of TR and FDE, the first 10^4 bits have higher BER than the bits after the DD-LMS updating algorithm works. However, due to the limitation of computational complexity, the interleaver for tens of thousands of bits is impractical, and thus cannot average the BER. Therefore, the BER versus ROP for the first 10^4 bits can determine the required ROP at the 20% FEC limit. More error bits appear when the ZF-based channel estimation is used. The tap coefficients initialized by the MMSE-based channel estimation are more accurate than those initialized by the ZF-based channel estimation.

Figures 4(e) and (f) show the BER versus ROP of the first 10^4 bits using ZF-based and MMSE-based channel estimations after optical back-to-back (OBtB) or 20km SSMF transmission. After the OBtB transmission, the BER can achieve the 20% FEC limit at the ROP of ~ -19dBm when the ZF-based channel estimation is used. When the MMSE-based channel estimation is used, the BER can achieve the 20% FEC limit at the ROP of ~ -20.5dBm. After 20km SSMF transmission, the BER can achieve the 20% FEC limit at the ROP of ~ -19dBm when the ZF-based channel estimation is used. When the MMSE-based channel estimation is used, the BER can achieve the 20% FEC limit at the ROP of ~ -20dBm. The BER performance is almost the same as that after the OBtB transmission because the zero-dispersion wavelength is chosen. Therefore, MMSE-based channel estimation has $\sim$ 1dB ROP benefit compared to ZF-based channel estimation.

4. Conclusions

In this paper, we propose the burst-mode DSP based on the designed preamble to achieve fast convergence for 50G DMT PON. The initial timing offset can be calculated using the designed frequency tones for the burst-mode TR. Meanwhile, the initial tap coefficients are estimated by the MMSE-based channel estimation for burst-mode FDE. The experimental results show that the burst-mode DSP can be converged using a short preamble within 27ns. The ROP can

Optics EXPRESS

be ~ −20dBm at the 20% FEC limit. Based on the burst-mode DSP, the DMT PON is more competitive for non-residential P2MP applications.

Funding. National Key Research and Development Program of China (2023YFB2905700); National Natural Science Foundation of China (62371207, 62005102); Young Elite Scientists Sponsorship Program by CAST (2023QNRC001); Hong Kong Research Grants Council GRF (15231923).

Disclosures. The authors declare no conflicts of interest.

Data availability. Data underlying the results presented in this paper are not publicly available at this time but may be obtained from the authors upon reasonable request.

References

1. G. Simon, F. Saliou, A. Afonso, *et al.*, "200 Gb/s coherent point-to-multipoint coexistence with 50G-PON for next-generation optical access," IEEE Photonics Technol. Lett. **36**(10), 665–668 (2024).
2. X. Liu, "Enabling optical network technologies for 5G and beyond," J. Lightwave Technol. **40**(2), 358–367 (2022).
3. Y. Zhu and W. Hu, "Optical access networks for fixed and mobile applications [Invited Tutorial]," J. Opt. Commun. Netw. **16**(2), A118–A135 (2024).
4. R. Bonk, D. Geng, D. Khotimsky, *et al.*, "50G-PON: The First ITU-T Higher-Speed PON System," IEEE Commun. Mag. **60**(3), 48–54 (2022).
5. D. Zhang, D. Liu, X. Wu, *et al.*, "Progress of ITU-T higher speed passive optical network (50G-PON) standardization," J. Opt. Commun. Netw. **12**(10), D99–D108 (2020).
6. B. Li, K. Zhang, D. Zhang, *et al.*, "DSP enabled next generation 50G TDM-PON," J. Opt. Commun. Netw. **12**(9), D1–D8 (2020).
7. J. Zhou, J. He, X. Lu, *et al.*, "100G fine-granularity flexible-rate passive optical networks based on discrete multi-tone with PAPR optimization," J. Opt. Commun. Netw. **14**(11), 944–950 (2022).
8. J. Zhou, L. Li, J. He, *et al.*, "Clipping discrete multi-tone for peak-power-constraint IM/DD optical systems," Sci. China Inf. Sci. **66**(5), 152302 (2023).
9. G. Liu, J. Zhou, Y. Huang, *et al.*, "Flexible transceiver for an access network: a multicarrier entropy loading approach," J. Opt. Commun. Netw. **15**(7), 442–448 (2023).
10. D. van Veen, A. Mahadevan, M. Straub, *et al.*, "Benefits of flexibility in current and future IM-DD based TDM-PON," J. Opt. Commun. Netw. **16**(7), C113–C120 (2024).
11. G. Simon, F. Saliou, J. Potet, *et al.*, "Assessment of training patterns performances in the context of burst mode equalization for 50G-PON," in *49th European Conference on Optical Communications*, (2023), pp. 151–154.
12. J. Li, N. Wang, J. Zhu, *et al.*, "First Real-Time Symmetric 50G TDM-PON Prototype with High Bandwidth and Low Latency," in *Opto-Electronics and Communications Conference (OECC)*, (2023), pp. 1–4.
13. J. Zhang, Q. Zhou, M. Zhu, *et al.*, "Demonstration of all-digital burst clock and data recovery for symmetrical 50 Gb/s/λ PON based on low-bandwidth optics," Opt. Commun. **516**, 128266 (2022).
14. P. Torres-Ferrera, H. Wang, V. Ferrero, *et al.*, "Optimization of band-limited DSP-aided 25 and 50 Gb/s PON using 10G-class DML and APD," J. Lightwave Technol. **38**(3), 608–618 (2020).
15. F. J. Effenberger, H. Zeng, A. Shen, *et al.*, "Burst-mode error distribution and mitigation in DSP-assisted high-speed PONs," J. Lightwave Technol. **38**(4), 754–760 (2020).
16. G. Simon, F. Saliou, J. Potet, *et al.*, "Assessment of training patterns performances in the context of burst mode equalization for 50G-PON," in *49th European Conference on Optical Communications (ECOC 2023)*, vol. 2023 (IET, 2023), pp. 151–154.
17. G. Coudyzer, P. Ossieur, L. Breyne, *et al.*, "Study of burst-mode adaptive equalization for> 25G PON applications," J. Opt. Commun. Netw. **12**(1), A104–A112 (2020).
18. V. E. Houtsma and D. T. van Veen, "Investigation of modulation schemes for flexible line-rate high-speed TDM-PON," J. Lightwave Technol. **38**(12), 3261–3267 (2020).
19. H. Wang, J. Zhou, Z. Xing, *et al.*, "Fast-convergence digital signal processing for coherent PON using digital SCM," J. Lightwave Technol. **41**(14), 4635–4643 (2023).
20. J. Zhou, Z. Xing, H. Wang, *et al.*, "Flexible Coherent Optical Access: Architectures, Algorithms, and Demonstrations," J. Lightwave Technol. **42**(16), C1 (2024).
21. C. Yang, R. Hu, M. Luo, *et al.*, "IM/DD-based 112-Gb/s/lambda PAM-4 transmission using 18-Gbps DML," IEEE Photonics J. **8**(3), 1–7 (2016).
22. Y. Ding, T. N. Davidson, Z.-Q. Luo, *et al.*, "Minimum BER block precoders for zero-forcing equalization," IEEE Trans. Signal Process. **51**(9), 2410–2423 (2003).
23. P. Monsen, "MMSE equalization of interference on fading diversity channels," IEEE Trans. Commun. **32**(1), 5–12 (1984).
24. W. Mo, J. Zhou, G. Liu, *et al.*, "Simplified LDPC-assisted CNC algorithm for entropy-loaded discrete multi-tone in a 100G flexible-rate PON," Opt. Express **31**(4), 6956–6964 (2023).
25. H. Cui, J. Zhou, W. Mo, *et al.*, "Flexible-rate PON based on entropy-loading DMT with wide-range adjustment from 12.5 to 87.5 Gbps," IEEE Photonics Technol. Lett. **36**(9), 609–612 (2024).
26. K. Wang, L. Zhang, Y. Chen, *et al.*, "FPGA-based 4× 29.4912 Gbit/s PS-PAM4 signal transmission with a low-complexity probabilistic shaping scheme," Opt. Lett. **48**(6), 1514–1517 (2023).